Available online at www.sciencedirect.com

ScienceDirect

Advances in Space Research 59 (2017) 917–935

ADVANCES IN SPACE RESEARCH (a COSPAR publication)

www.elsevier.com/locate/asr

Characterisation of Special Sensor Microwave Water Vapor Profiler (SSM/T-2) radiances using radiative transfer simulations from global atmospheric reanalyses

Shinya Kobayashi [a,*], Paul Poli [b,1], Viju O. John [c,d]

[a] Japan Meteorological Agency, 1-3-4 Otemachi, Chiyoda-ku, Tokyo 100-8122, Japan
[b] Météo-France Centre de Météorologie Marine, 13 rue du Chatellier, CS 12804, 29228 Brest Cedex 2, France
[c] Met Office Hadley Centre, FitzRoy Road, Exeter EX1 3PB, UK
[d] European Organisation for the Exploitation of Meteorological Satellites, Eumetsat Allee 1, D-64295 Darmstadt, Germany

Received 23 June 2016; received in revised form 10 November 2016; accepted 11 November 2016
Available online 18 November 2016

Abstract

The near-global and all-sky coverage of satellite observations from microwave humidity sounders operating in the 183 GHz band complement radiosonde and aircraft observations and satellite infrared clear-sky observations. The Special Sensor Microwave Water Vapor Profiler (SSM/T-2) of the Defense Meteorological Satellite Program began operations late 1991. It has been followed by several other microwave humidity sounders, continuing today. However, expertise and accrued knowledge regarding the SSM/T-2 data record is limited because it has remained underused for climate applications and reanalyses. In this study, SSM/T-2 radiances are characterised using several global atmospheric reanalyses. The European Centre for Medium-Range Weather Forecasts (ECMWF) Interim Reanalysis (ERA-Interim), the first ECMWF reanalysis of the 20th-century (ERA-20C), and the Japanese 55-year Reanalysis (JRA-55) are projected into SSM/T-2 radiance space using a fast radiative transfer model. The present study confirms earlier indications that the polarisation state of SSM/T-2 antenna is horizontal (not vertical) in the limit of nadir viewing. The study also formulates several recommendations to improve use of the SSM/T-2 measurement data in future fundamental climate data records or reanalyses. Recommendations are (1) to correct geolocation errors, especially for DMSP 14; (2) to blacklist poor quality data identified in the paper; (3) to correct for inter-satellite biases, estimated here on the order of 1 K, by applying an inter-satellite recalibration or, for reanalysis, an automated (e.g., variational) bias correction; and (4) to improve precipitating cloud filtering or, for reanalysis, consider an all-sky assimilation scheme where radiative transfer simulations account for the scattering effect of hydrometeors.

Keywords: Upper tropospheric humidity; Microwave humidity sounder; Reanalysis; Climate monitoring; Data assimilation; Radiative transfer

1. Introduction

Water vapour plays an important role in regulating the energy balance of the Earth's atmosphere. It provides a key feedback in the greenhouse effect, and is essential to the formation of clouds and precipitation (Hartmann et al., 2013), and is identified as an Essential Climate Variable (ECV) by the Global Climate Observing System (GCOS, 2010). Long-term high-quality Climate Data Records (CDRs) of this ECV are required to understand the feedback mechanism and monitor its variability.

In situ measurements of this ECV have been collected since the first half of the 20th century, from weather

* Corresponding author.
E-mail addresses: s-kobayashi@met.kishou.go.jp (S. Kobayashi), paul.poli@shom.fr (P. Poli), viju.john@eumetsat.int (V.O. John).
[1] Previously at European Centre for Medium-Range Weather Forecasts, Shinfield Park, Reading RG2 9AX, UK.

http://dx.doi.org/10.1016/j.asr.2016.11.017

balloons or aircraft (Stickler et al., 2010), however the spatial coverage is mostly limited to land. From satellites, atmospheric upper tropospheric humidity can be estimated thanks to its spectral signature on measurements of atmospheric radiation, in the microwave and other parts of the electromagnetic spectrum. From the nadir view, vertical soundings can be obtained by sampling the spectrum at different frequencies. Humidity retrievals have mostly focused on the troposphere, because tropospheric water vapour is far more abundant than in the stratosphere and because early instruments had higher measurement noise and lower spectral resolution.

Unlike infrared sounders whose measurements do not penetrate through clouds, microwave humidity sounders sampling the 183.31 GHz water vapour rotational-transition band provide almost global and all-sky coverage of tropospheric humidity, except in precipitating cloud conditions. Consequently, microwave humidity sounders have the potential to complement, for tropospheric humidity, the coverage limitations of the other existing data records, which are in situ and/or satellite-infrared-based (e.g. John et al., 2011).

Nearly 20 microwave humidity sounders have been flown and used for Numerical Weather Prediction (NWP) applications since 1998 (Table 1). There are commitments to continue the operational sensing capability: additional Microwave Humidity Sounder (MHS; Robel, 2009) on the European Organisation for the Exploitation of Meteorological Satellites (EUMETSAT) Polar System (EPS) Metop satellites, Microwave Humidity Sounder (MWHS; Chen et al., 2015) on the Chinese Feng-Yun-3 (FY-3) satellites and Imaging/Sounding Microwave Radiometer-improved (MTVZA-GY; Gorobets et al., 2007) on the Russian Meteor-M satellites, are planned on subsequent satellites of their respective series; additional Advanced Technology Microwave Sounder (ATMS; Weng et al., 2013) will also fly on satellites of the U.S. Joint Polar Satellite System (JPSS); the Microwave Sounder (MWS) will fly on the European Metop-Second Generation (Metop-SG) satellites. Overall, these plans cover timeframes as far as the year 2040, continuing records that started in mid-1998.

However, observations by microwave humidity sounders began earlier, with the Special Sensor Microwave Water Vapor Profiler (SSM/T-2), whose first instance was launched on 28 November 1991. Four satellites in the U. S. Defense Meteorological Satellite Program (DMSP), the longest-running meteorological satellite program to date, carried SSM/T-2 instruments: 3 Block 5D-2 satellites (DMSP 11, 12, and 14, respectively COSPAR designation 1991-082A, 1994-057A, and 1997-012A) and the first Block 5D-3 satellite (DMSP 15, COSPAR 1999-067A).

The SSM/T-2 radiance data are hence key to extend backward the microwave sounding record by about 6 years. In light of a (currently) 18-year-long record of microwave humidity sounding, these few additional years are of critical importance to improve the potential resulting CDR of tropospheric humidity. Creating such a CDR from the SSM/T-2 data requires first the creation of a Fundamental Climate Data Record (FCDR) of error-characterised and bias-adjusted SSM/T-2 radiances.

Apart from SSM/T-2, most data collected by instruments listed in Table 1 have been used in the NWP community, and the error characteristics of these measurements are known to some extent. In contrast, the SSM/T-2 data have remained underused both for NWP and for climate applications. Consequently, expertise with using these data is limited. In order to quantitatively assess error characteristics of the SSM/T-2 data, high quality reference data are necessary for validation. However, such observations are rarely available, especially for the period before 1998 when the Advanced Microwave Sounding Unit (AMSU)-B observations began. An alternative approach is to compare with equivalent brightness temperatures computed from a realistic NWP or reanalysis system. The latest fast radiative transfer models, such as for example the Radiative Transfer for the TIROS Operational Vertical Sounder (RTTOV; Saunders et al., 2013), are capable of simulating brightness temperatures with high accuracy in clear sky conditions, which can be used as reliable reference data to evaluate the instrument biases. Several useful insights on characterisations of satellite microwave instruments have been obtained from differences between observations and estimates from NWP systems (e.g. Lu et al., 2011; Lu and Bell, 2014) and reanalyses (e.g. Poli et al., 2015).

The paper presents results of characterisation of SSM/T-2 radiances using several global atmospheric reanalyses. The European Centre for Medium-Range Weather Forecasts (ECMWF) Interim Reanalysis (ERA-Interim; Dee et al., 2011), the first ECMWF reanalysis of the 20th-century (ERA-20C; Poli et al., 2016), and the Japanese 55-year Reanalysis (JRA-55; Kobayashi et al., 2015a) are compared to SSM/T-2 by means of fast radiative transfer calculations in clear sky conditions. The SSM/T-2 data record and reanalysis datasets are outlined in Section 2. The radiative transfer calculations and comparison methodology are presented in Section 3. Improved quality controls of SSM/T-2 data are proposed in Section 4. Section 5 reviews the error characteristics of SSM/T-2 measurements. Conclusions and recommendations are presented in Section 6.

2. Data

2.1. SSM/T-2

The SSM/T-2 instrument is a five-channel passive microwave sensor operating in the 90–190 GHz frequency region (Galin et al., 1993). Three channels sample the emission in the 183.31 GHz band for atmospheric water vapour profile retrievals, at ±1 GHz (channel 2), ±3 GHz (channel 1), and ±7 GHz (channel 3), enabling to sense (respectively) the Upper Tropospheric Humidity (UTH), the Mid Tropospheric Humidity (MTH), and the Lower Tropospheric Humidity (LTH). Two other channels sense near

Table 1
Channel characteristics for microwave humidity sounders that have been flown on meteorological satellites.

Ch	Centre frequency (GHz)	No of passbands	Band width per passband (GHz)	NEΔT (K)[a]	Polarisation angle[b]	IFOV[c] (km)
SSM/T-2 (Special Sensor Microwave Water Vapor Profiler) (Galin et al., 1993) *on the DMSP (Defense Meteorological Satellite Program) satellites, 1992–2008*						
4	91.655 ± 1.25	2	1.5	0.60	H	88 (nadir)
5	150.0 ± 1.25	2	1.5	0.60	H	54 (nadir)
2	183.31 ± 1.0	2	0.5	0.80	H	48 (nadir)
1	183.31 ± 3.0	2	1.0	0.60	H	48 (nadir)
3	183.31 ± 7.0	2	1.5	0.60	H	48 (nadir)
AMSU-B (Advanced Microwave Sounding Unit-B) (Robel, 2009) *on NOAA (National Oceanic and Atmospheric Administration) POES (Polar Orbiting Environmental Satellites), 1998–2014*						
1	89.0	2	1.0	0.37	V	16.3 (nadir)
2	150.0	2	1.0	0.84	V	16.3 (nadir)
3	183.31 ± 1.00	2	0.5	1.06	V	16.3 (nadir)
4	183.31 ± 3.00	2	1.0	0.70	V	16.3 (nadir)
e	183.31 ± 7.00	2	2.0	0.60	V	16.3 (nadir)
SSMIS (Special Sensor Microwave Imager/Sounder) (Kunkee et al., 2008a) *on DMSP, 2003-present*						
17	91.655	2	1.418 [d]	0.33	V*	12.5 [e]
18	91.655	2	1.411 [d]	0.32	H*	12.5 [e]
8	150	2	1.642 [d]	0.89	H*	12.5 [e]
11	183.31 ± 1	2	0.513 [d]	0.81	H*	12.5 [e]
10	183.31 ± 3	2	1.019 [d]	0.67	H*	12.5 [e]
9	183.31 ± 6.6	2	1.526 [d]	0.97	H*	12.5 [e]
MHS (Microwave Humidity Sounder) (Robel, 2009) *on NOAA POES and EPS (EUMETSAT (European Organisation for the Exploitation of Meteorological Satellites) Polar System) Metop, 2005-present*						
1	89.0	1	2.4	0.22	V	16.3 (nadir)
2	157.0	1	2.4	0.34	V	16.3 (nadir)
3	183.311 ± 1.0	2	0.5	0.51	H	16.3 (nadir)
4	183.311 ± 3.0	2	0.9	0.40	H	16.3 (nadir)
5	190.311	1	2.2	0.46	V	16.3 (nadir)
MWHS (Microwave Humidity Sounder) (Chen et al., 2015) *on FY-3 (Feng-Yun-3), 2008-present*						
1	150	2	1.0	0.9	V	15 (nadir)
2	150	2	1.0	0.9	H	15 (nadir)
3	183.31 ± 1	2	0.5	1.1	V	15 (nadir)
4	183.31 ± 3	2	1.0	0.9	V	15 (nadir)
5	183.31 ± 7	2	1.0	0.9	V	15 (nadir)
MTVZA-GY (Imaging/Sounding Microwave Radiometer-improved) (Gorobets et al., 2007) *on Meteor-M, 2009-present*						
25	91.65	2	2.5	0.6	V*	14 × 30
26	91.65	2	2.5	0.6	H*	14 × 30
29	183.31 ± 1.0	2	0.5	0.5	V*	9 × 21
28	183.31 ± 3.0	2	1.0	0.6	V*	9 × 21
27	183.31 ± 7.0	2	1.5	0.8	V*	9 × 21
ATMS (Advanced Technology Microwave Sounder) (Weng et al., 2013) *on the Suomi NPP (National Polar-orbiting Partnership) satellite, 2011-present*						
16	88.2	1	2.0	0.50	V	32.6 (nadir)
17	165.5	1	3.0	0.60	H	16.3 (nadir)
22	183.31 ± 1.0	2	0.5	0.90	H	16.3 (nadir)
20	183.31 ± 3.0	2	1.0	0.80	H	16.3 (nadir)
18	183.31 ± 7.0	2	2.0	0.80	H	16.3 (nadir)
SAPHIR (Sondeur Atmosphérique du Profil d'Humidité Intertropicale par Radiométrie) (Roca et al., 2015) *on Megha-Tropiques, 2011-present*						
1	183.31 ± 0.2	2	0.2	2.4	V	10 (nadir)
2	183.31 ± 1.1	2	0.35	1.8	V	10 (nadir)
3	183.31 ± 2.8	2	0.5	1.8	V	10 (nadir)
4	183.31 ± 4.2	2	0.7	1.5	V	10 (nadir)
5	183.31 ± 6.6	2	1.2	1.5	V	10 (nadir)
6	183.31 ± 11.0	2	2.0	1.2	V	10 (nadir)
GMI (Global Precipitation Measurement (GPM) Microwave Imager) (Draper et al., 2015) *on GPM, 2014-present*						
8	89.0	2	2.735 [f]	0.32	V*	4.4 × 7.3
9	89.0	2	2.758 [f]	0.31	H*	4.4 × 7.3
10	166	2	1.569 [f]	0.7	V*	4.4 × 7.3
11	166	2	1.601 [f]	0.65	H*	4.4 × 7.3

(*continued on next page*)

Table 1 (*continued*)

Ch	Centre frequency (GHz)	No of passbands	Band width per passband (GHz)	NEΔT (K)[a]	Polarisation angle[b]	IFOV[c] (km)
12	183.31 ± 3	2	1.482 [f]	0.56	V*	4.4 × 7.3
13	183.31 ± 7	2	1.874 [f]	0.47	V*	4.4 × 7.3

[a] Noise Equivalent Delta Temperature; Values from specification for SSM/T-2 and SAPHIR, from NOAA-15 for AMSU-B, from DMSP 16 for SSMIS, from NOAA-18 for MHS, from FY-3A for MWHS, from Meteor-M N2 for MTVZA-GY, from Suomi NPP for ATMS, and from the GPM Core satellite for GMI.

[b] The V and H polarisations correspond respectively to electrical fields normal or parallel to the ground track at nadir (rotating by an angle equal to the scan angle for off-nadir directions, except for conical scanners indicated by *).

[c] Instantaneous Field-Of-View.

[d] Values from DMSP 16 for SSMIS.

[e] Sampling interval along scan direction based on 833 km spacecraft altitude.

[f] Values from the GPM Core satellite for GMI.

the 91 GHz (channel 4) and 150 GHz (channel 5) frequencies.

As indicated in the introduction, this microwave humidity sounder, flown on 4 DMSP satellites (DMSP 11, 12, 14 and 15), started the operational monitoring of the 183 GHz frequency from space. Emission at or near the other low-frequency water vapour rotational-transition band of 22.23 GHz, was sensed as early as 1972 by the Microwave Spectrometer (NEMS) on Nimbus-5, followed by the Scanning Microwave Spectrometer (SCAMS) on Nimbus-6, the Scanning Multichannel Microwave Radiometer (SMMR) on Nimbus-7 and Seasat, the Special Sensor Microwave/Imager (SSM/I) on several DMSP satellites after 1987, and several Microwave Radiometer (MWR) instruments employed in conjunction with sea-level altimeters on, e.g., European Remote Sensing Satellites (ERS)-1, and -2, Envisat, Jason-1, -2 and -3, but also Russian satellites of the Okean series (WMO, 2016). However, given radiometric capabilities, the 22 GHz line is not strong enough to allow sub-sampling, and hence measurements at this frequency or nearby only allow retrieving total column water, and no vertical profile (Kakar, 1983).

The SSM/T-2 data considered in this study cover the period from 1992 to 2008. Fig. 1 shows the temporal coverage of each of the SSM/T-2 instruments. Prior to this study, the full set of SSM/T-2 antenna temperatures were obtained originally from the U.S. National Oceanic and Atmospheric Administration (NOAA) National Geophysical Data Center (NGDC) and converted into the NetCDF format with some additional quality information (John and Chung, 2014). In the present study, we further convert the data into the ODB format and archive them into the ECMWF Meteorological Archive and Retrieval System (MARS) archive. A detailed list of parameters in SSM/T-2 ODB files and access instructions to those files are given in Kobayashi et al. (2015b). It should be noted that antenna pattern corrections are not performed, hence the results obtained in this study are relevant to the antenna temperature. These antenna temperatures are directly compared to simulated brightness temperatures, and both data are referred to as "brightness temperatures" throughout this paper for brevity. In radiative transfer simulations, antennas are assumed to have the perfect directivity and reflectivity, but in reality they do not: they have a minor sensitivity to undesired directions, and their reflectivities are less than unity. These characteristics can be potential sources of discrepancy between observations and simulations.

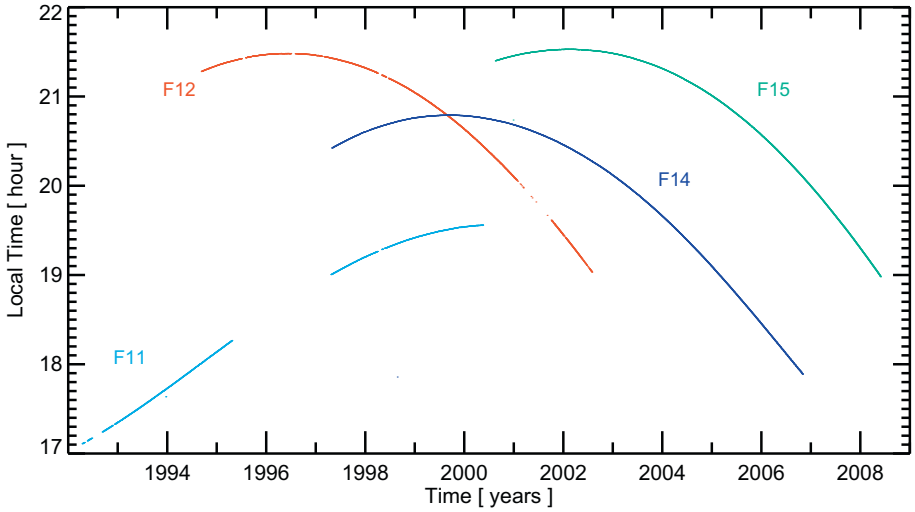

Fig. 1. Equator crossing times of the ascending nodes of the DMSP satellites that have SSM/T-2 instruments on-board. Values are plotted only for the periods during which SSM/T-2 data are available for this study.

Table 1 shows channel characteristics for SSM/T-2 and the other instruments mentioned earlier, measuring radiation near the 183.31 GHz band of water vapour. Note that SSM/T-2 has larger fields of view (FOVs) than the others. Channels 1–3 of SSM/T-2 are the tropospheric humidity profiling channels; channels 4 and 5 are window channels and are used to filter rainy scenes (Ferraro et al., 2000) which obfuscate retrieval of tropospheric humidity.

2.2. Reanalysis data

In the absence of global in situ humidity data, spatio-temporally complete reanalysis data are used for comparison with SSM/T-2. The ERA-Interim reanalysis data are used at 6-hourly temporal resolution, on the native model grid at Gaussian grid truncation 255 (about 79 km horizontal resolution). Data include profiles of temperature and specific humidity on 60 model levels and the following surface parameters: surface pressure, land/sea mask, skin temperature, 10-m eastward and northward wind components, surface geopotential, 2-m temperature and dewpoint, and sea ice fraction.

In order to assess the stability of SSM/T-2 measurements, it is important to consider the temporal consistency as well as the instantaneous accuracy of the reanalysis data. ERA-Interim arguably maintains better temporal consistency of the upper tropospheric humidity compared with other recent comprehensive reanalyses (e.g., Chung et al., 2016). However, there are in fact several known issues with temporal jumps in the representation of the water cycle in ERA-Interim (e.g., Dee et al., 2011). Accordingly, radiative transfer simulations are also performed from two other reanalyses, ERA-20C and JRA-55. ERA-20C adopted an approach of a fixed observing system to achieve a higher level of temporal consistency where only surface pressure and marine wind observations were assimilated (Poli et al., 2016). In contrast, JRA-55 is a comprehensive reanalysis like ERA-Interim, which assimilated as many observations as possible from various sources including satellite observing systems to achieve a higher instantaneous accuracy. Although JRA-55 suffers a dry bias of the forecast model in the upper and mid troposphere, the bias is mostly constrained for the period after 2000 during which a large number of observations from satellite water vapour channels were assimilated (Kobayashi et al., 2015a).

3. Methodology

The reanalysis geophysical data are first interpolated in the horizontal domain to the SSM/T-2 observation location. Temporal interpolation is not performed; instead, the reanalysis data that are closest in time are used. The interpolated geophysical parameters are then input to the radiative transfer model to calculate equivalent brightness temperatures.

Fast radiative transfer calculations are conducted with RTTOV version 11.2 (Saunders et al., 2013). The radiative transfer coefficients for SSM/T-2 were supplied by the EUMETSAT Satellite Application Facility on Numerical Weather Prediction (NWP SAF). Surface emissivities are estimated with the Fast Microwave Emissivity Model (FASTEM)-5 (Liu et al., 2011) over sea, and assumed to be 0.95 over land and 0.90 over sea-ice.

Since the emission from the ocean surface is polarised, observed radiances vary considerably with the direction of polarisation especially for surface-sensitive channels. However, the polarisation state of the SSM/T-2 can be qualified as unspecified: it rotates by an angle equal to the scan angle, but some publications assume *vertical* polarisation at nadir (e.g. Felde and Pickle, 1995), while others assume *horizontal* polarisation at nadir (e.g. Wessel and Boucher, 1998). Burns et al. (1998) investigated this "unspecified" polarisation state by comparing observations and simulations, and concluded that the antenna was oriented towards horizontal polarisation in the limit of nadir viewing. This result was corroborated by information from the Aerojet system engineer for the SSM/T-2 project (Burns et al., 1998). A comparison between observations and simulations from window channels in Fig. 2 demonstrates that assuming vertical polarisation at nadir results in large scan angle dependent biases that are symmetrical with respect to nadir. However, assuming horizontal polarisation at nadir almost completely removes the scan angle dependent biases. Based on this finding, radiative transfer simulations presented thereafter assume horizontal polarisation at nadir.

Regarding the centre frequency of channel 4, some documents indicate 91.655 GHz (e.g. Galin et al., 1993) whereas others indicate 91.665 GHz (e.g. Falcone et al., 1992). Since the tropospheric humidity channels (1–3) share a single local oscillator with one of the window channel (4) by using the doubled frequency (183.31 GHz) (Galin et al., 1993), the correct centre frequency of channel 4 should be 91.655 GHz. Accordingly, the radiative transfer coefficients used in the present study assume 91.655 GHz.

Since the SSM/T-2 data record does not contain satellite zenith angles that are necessary for radiative transfer simulations, they are computed from satellite altitudes, nominal nadir angles (out to 40.5 degrees on both sides of the swath, spaced by 3 degrees), and the Earth's radius as an ellipsoid of revolution. Surface elevation is not taken into account, which leads to slightly overestimated satellite zenith angles over high terrain, but errors arising from this issue are minor (around 0.1% at the outermost scan position for the altitude of 5000 m).

4. Improved quality controls

4.1. Geolocation

Geolocation errors are one of the main sources of uncertainty in satellite microwave observations and have serious

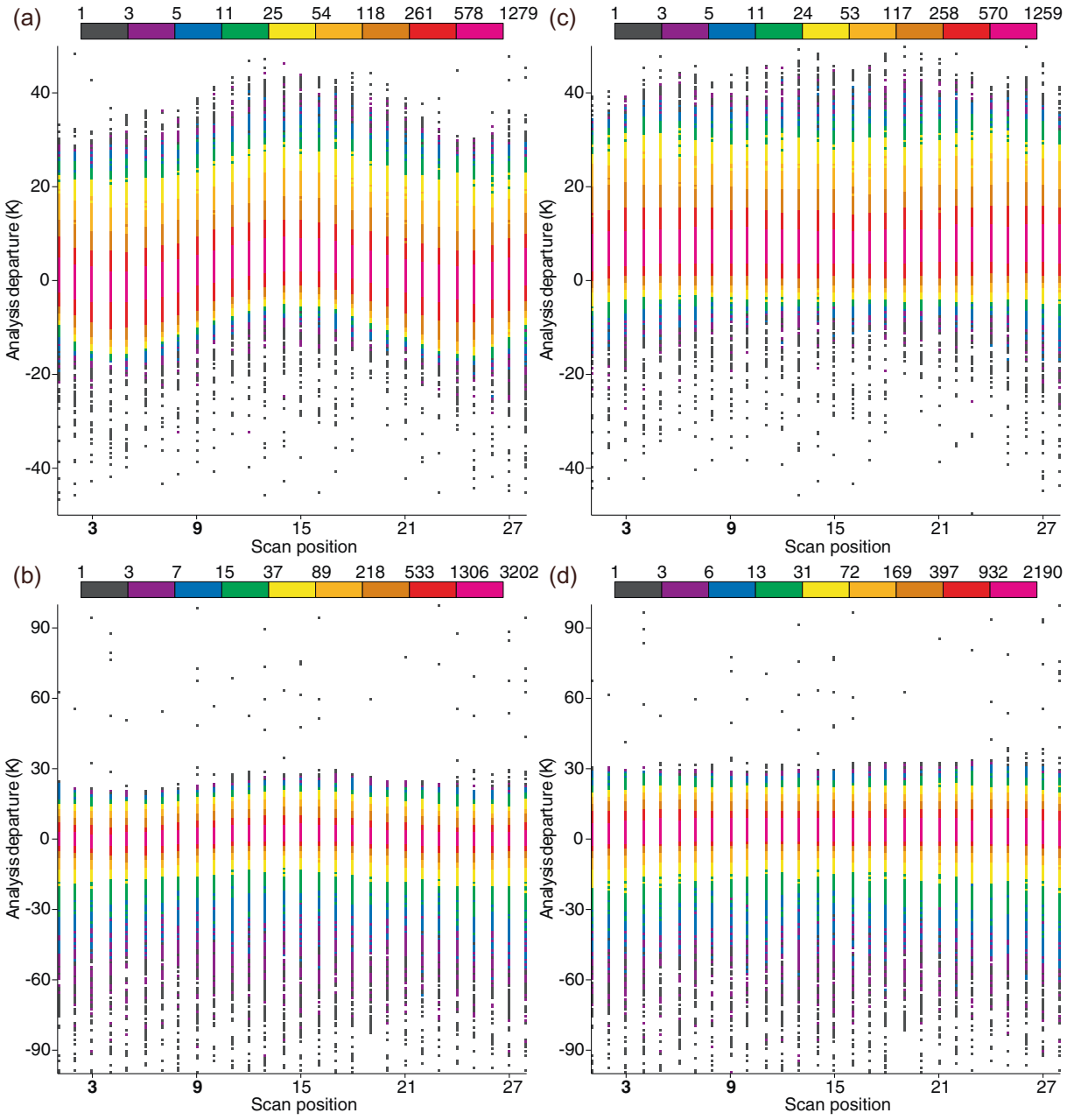

Fig. 2. Scatter density plots between scan position and analysis departure for (a, c) channel 4 (91 GHz) and (b, d) channel 5 (150 GHz) of SSM/T-2 on DMSP 12. Polarisation at nadir is assumed to be vertical in (a, b) and horizontal in (c, d). The statistics are computed using the data over sea from 31 December 2000, 21 UTC to 8 January 2001, 21 UTC, using ERA-Interim profiles as input to the radiative transfer simulations.

effects on inter-calibrating, validating and retrieving geophysical variables from them (Moradi et al., 2013). Since there is a large difference between surface emissivities over land and sea in the microwave frequencies, large geolocation errors lead to erroneous surface emissivities being used in radiative transfer simulations for observations near shorelines and result in distinctive departures of window channels, which have large sensitivities to the surface. Fig. 3 shows departures from the ERA-Interim analysis for channel 4 of SSM/T-2 on each satellite. Among these satellites, DMSP 14 exhibits especially large departures along shorelines with opposite signs in east and west coasts, which is a pattern that emerges when there are roll errors in the spacecraft attitude or sensor mounting for polar orbiting satellites.

Berg et al. (2013) corrected geolocation errors in data from the Special Sensor Microwave/Imager (SSM/I) on DMSP satellites using more accurate spacecraft ephemeris and sensor mounting angles estimated from differences between brightness temperatures of ascending and descending orbits to produce FCDRs from these data. A similar correction method might be applicable to the geolocation errors in SSM/T-2 data.

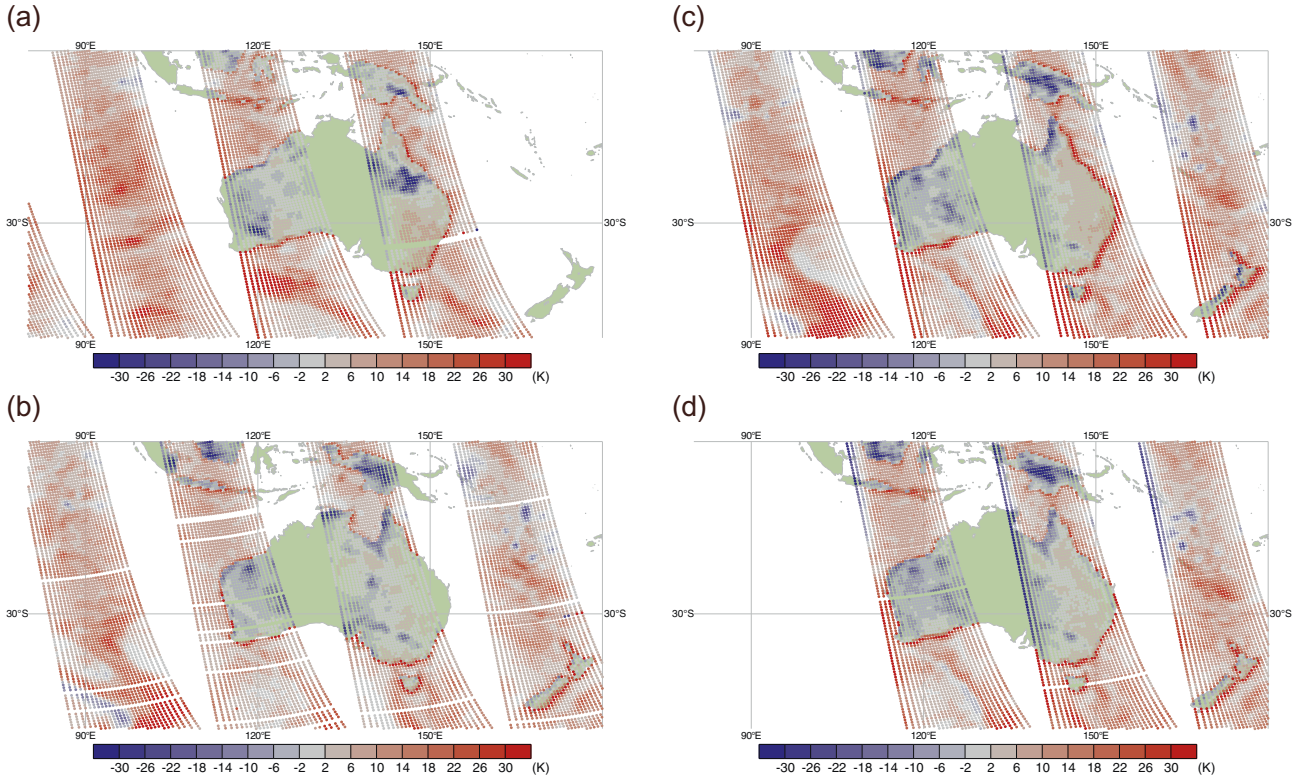

Fig. 3. Departures from the ERA-Interim analysis for channel 4 (91 GHz) of SSM/T-2 on (a) DMSP 11, (b) DMSP 12, (c) DMSP 14 and (d) DMSP 15. The data are for around 3 January 1999, 12 UTC for DMSP 11 and around 3 January 2001, 12 UTC for the others.

4.2. Scan-angle dependence

Some of the measurements at several outermost positions on the solar side of the SSM/T-2 were contaminated by the glare obstruction bracket, which was designed to keep sun light out of the instrument cavity (e.g. Miao et al., 2001). Fig. 4 shows scatter density plots between scan position and analysis departure for channel 2 of SSM/T-2 on each satellite. Significant effects of the interference from the glare obstructor can be found in measurements at the scan positions 26–28 on all satellites except DMSP 12.

Unless they can be corrected, these particular data should be excluded from further use. No similar effect is found for DMSP 12 and the cause of this difference, unknown at the moment, should be investigated. This may be understood from the satellite design, conducting graphical ray-tracing simulations as done by Kunkee et al. (2008b) for the Special Sensor Microwave Imager/Sounder (SSMIS) on DMSP 16 to understand the effect of this obstructor.

4.3. Visual inspection of maps

A visual inspection of maps suggest abnormal patterns during the time period before 1994. Observed data can be noisy because of the presence of clouds and other natural effects, so these anomalies are best shown by comparison with reanalyses. A quasi-regular stripe pattern is visible in maps in Fig. 5(a). This periodicity is due to the fact that the brightness temperature array in the SSM/T-2 data record contains a cluster of several corrupted data approximately every 70 elements (this irregularity varies slightly). This array has two dimensions of 28 scan positions by five channels. Thus, a large departure appears every 10 data points or so for each channel. The regularity of this problem is not found in the reanalysis data so it must originate in the observations. Quality flags in the SSM/T-2 data are not always set for these poor quality data (Fig. 5(b)). Therefore, an additional quality control, such as a departure check, is essential to remove these erroneous data (Fig. 5(c)).

5. Comparison between observed and simulated brightness temperatures

5.1. Cloud detection

Fig. 6 shows scatter density plots between observed and simulated brightness temperatures from each channel of SSM/T-2 on DMSP 15 over sea from 31 December 2000, 21 UTC to 7 January 2001, 21 UTC. During this period, radiances from AMSU-B were assimilated in ERA-Interim, and its tropospheric humidity analysis should be reasonably accurate. For DMSP 15, there is no major issue

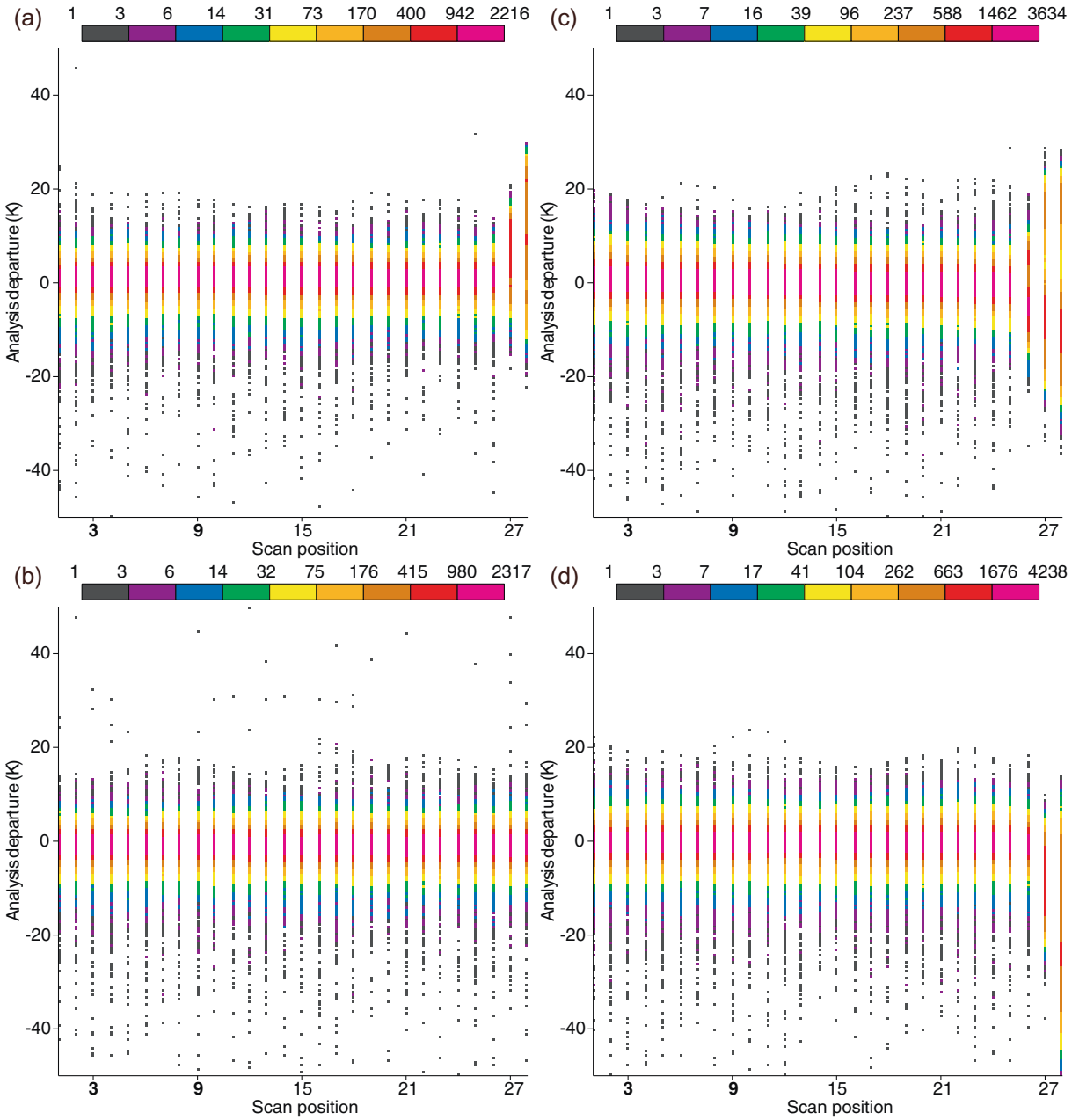

Fig. 4. Scatter density plots between scan position and analysis departure for channel 2 (UTH) of SSM/T-2 on (a) DMSP 11, (b) DMSP 12, (c) DMSP 14 and (d) DMSP 15. The statistics are computed using the data over sea from 31 December 1998, 21 UTC to 8 January 1999, 21 UTC for DMSP 11 and from 31 December 2000, 21 UTC to 7 January 2001, 21 UTC for the others, using ERA-Interim profiles as input to the radiative transfer simulations.

such as geolocation errors during this period. Thus, the quality control applied here is only to exclude measurements at the scan positions 26–28 as mentioned in Section 4.2. In the plots for tropospheric humidity channels (Fig. 6(a)–(c)) and the 150 GHz channel (Fig. 6(e)), some of the data are distributed off the diagonal on the left due to the fact that the scattering effect of hydrometeors such as cloud particles are not taken into account in the radiative transfer simulations.

To detect cloud-affected measurements, the cloud filtering method of Buehler et al. (2007) for AMSU-B is employed in this study. The method uses two criteria: a viewing angle (θ) dependent threshold on the brightness temperature at 183.31 ± 1.0 GHz (T_1^b), and a threshold on difference between the brightness temperature at 183.31 ± 3.0 GHz (T_3^b) and T_1^b. The former criterion is based on the fact that T_1^b should exceed around 240 K (for nadir looking measurements) in clear skies. In this study, we performed regression analysis on the values for AMSU-B (Buehler et al., 2007, Table 1) and derived a regression equation using a reciprocal direction cosine of the viewing angle (θ) as an independent variable (Eq. (1)). The latter criterion is derived from the fact that T_1^b is colder than T_3^b in clear skies due to the atmospheric temperature lapse rate, whereas T_1^b can be warmer than T_3^b in the presence of ice clouds. Specifically, measurements

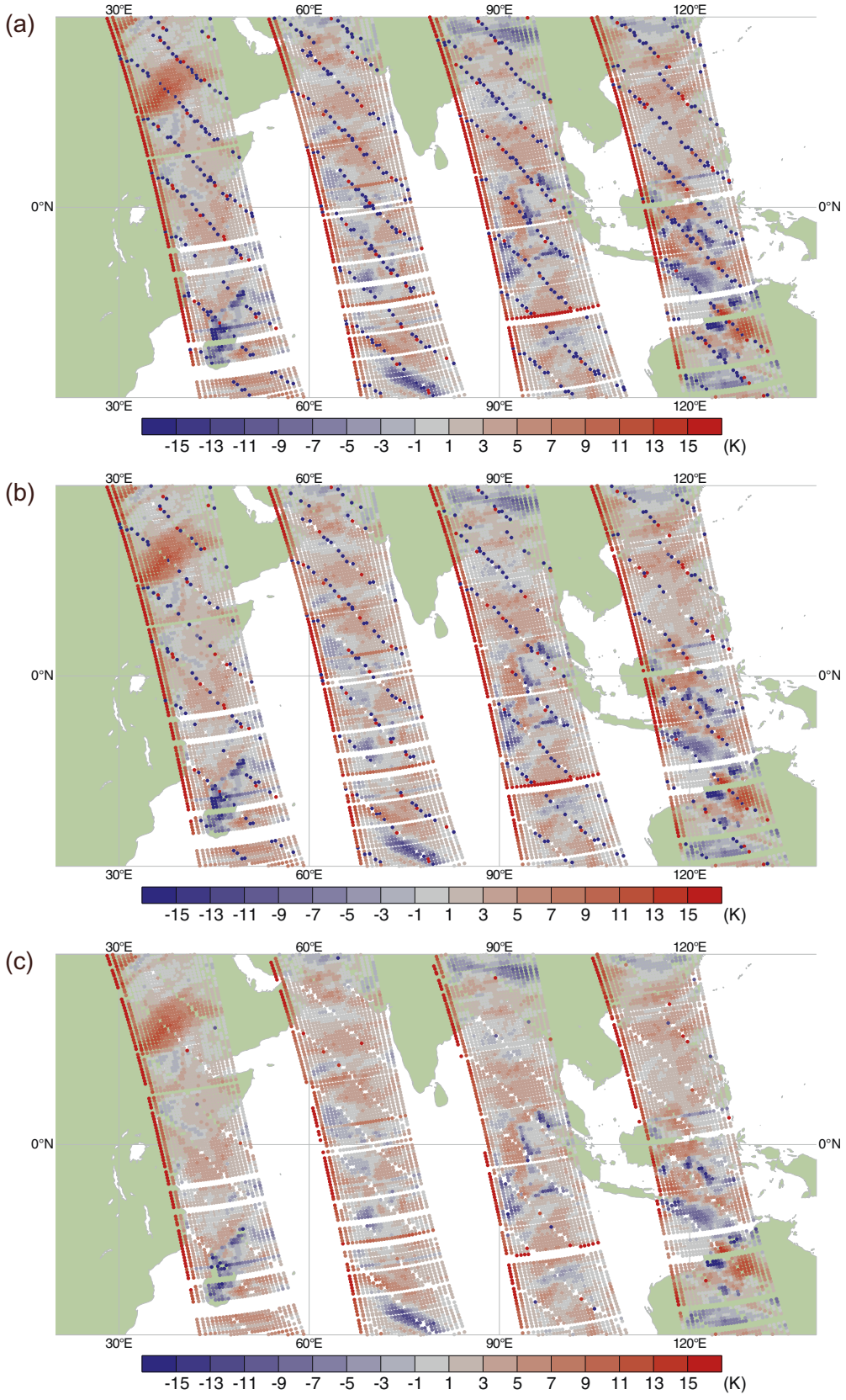

Fig. 5. Departures from the ERA-Interim analysis for channel 2 (UTH) of SSM/T-2 on DMSP 11 around 5 January 1993, 12 UTC. (a) All data, (b) those after quality flag check, and (c) those after quality flag check and departure check (±20 K).

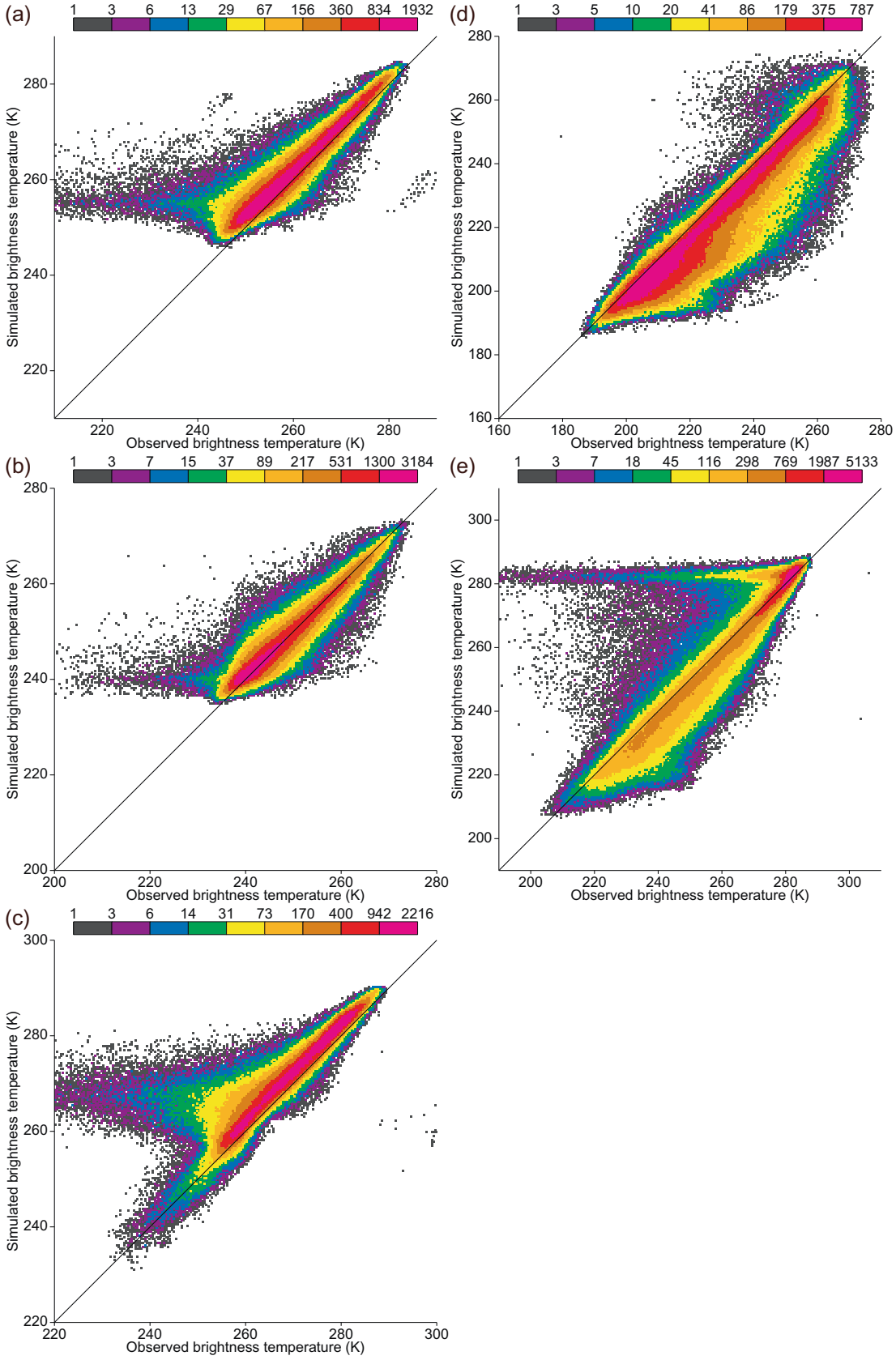

Fig. 6. Scatter density plots between observed and simulated brightness temperatures from (a) channel 1 (MTH), (b) channel 2 (UTH), (c) channel 3 (LTH), (d) channel 4 (91 GHz) and (e) channel 5 (150 GHz) of SSM/T-2 on DMSP 15 over sea from 31 December 2000, 21 UTC to 7 January 2001, 21 UTC before cloud filtering, using ERA-Interim profiles as input to the radiative transfer simulations.

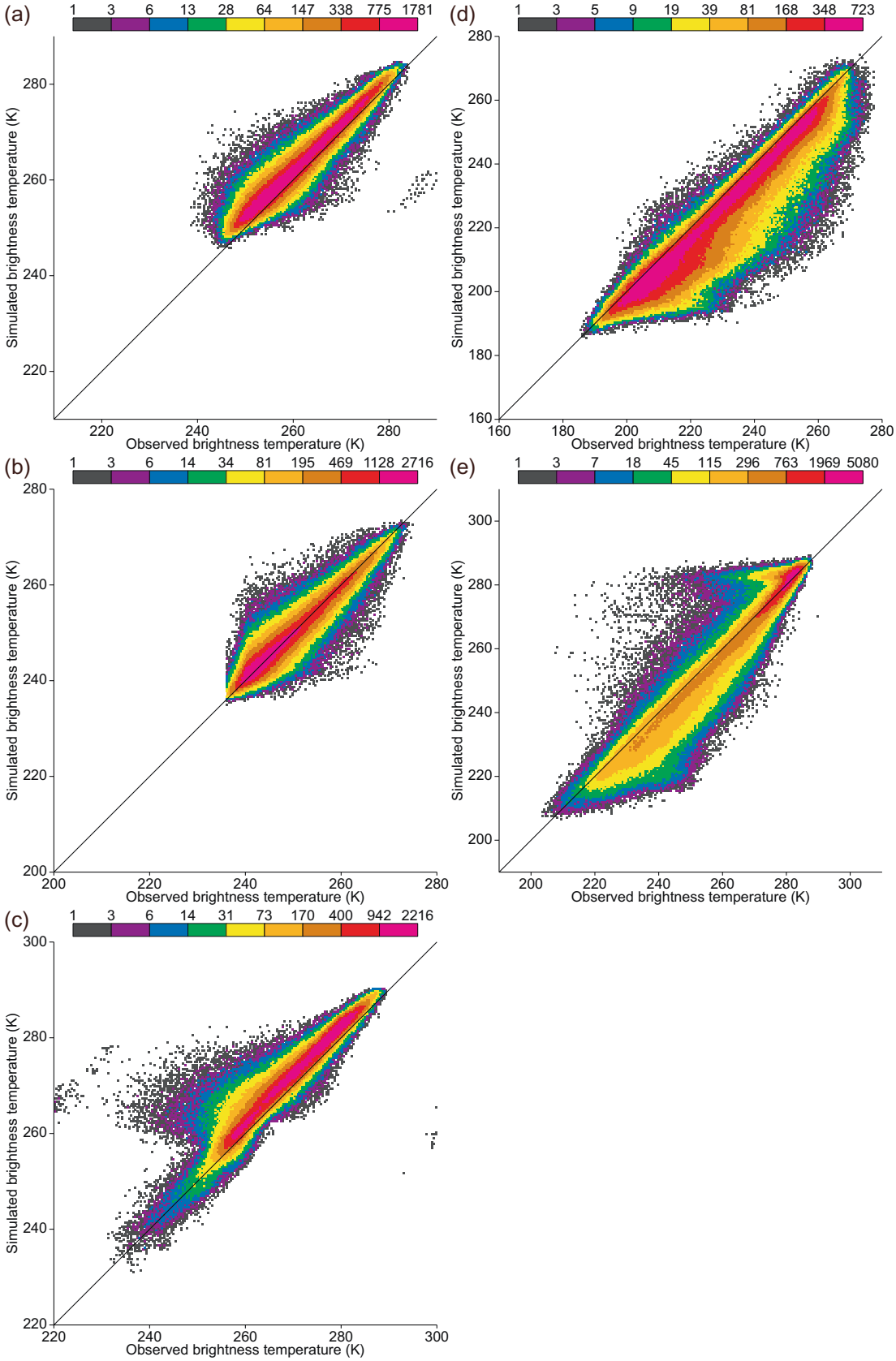

Fig. 7. As Fig. 6, but after cloud filtering.

satisfying either of the following criteria are considered affected by clouds in this study:

$$T_1^b \leqslant 252.49 - [12.395/\cos(\theta)] \quad (1)$$

$$T_3^b - T_1^b \leqslant 0.0 \quad (2)$$

Fig. 7 shows the same scatter density plots as Fig. 6 except that cloud-affected measurements, according to the test explained above, are excluded. The data that pass the cloud filtering are in general distributed along the diagonal. However, the distribution tends to be biased slightly to the left in the middle part for the lower tropospheric humidity channel (Fig. 7(c)) and in the upper part for the 150 GHz channel (Fig. 7(e)). Those measurements are most likely the ones affected by cloud particles or rain drops in the lower troposphere because the cloud filtering method of Buehler et al. (2007) is designed primarily for ice clouds in the upper troposphere. It can also be seen that simulated brightness temperatures for the 91.655 GHz channel are considerably lower than observations, indicating that radiances from the surface are underestimated in the radiative transfer simulations.

5.2. Attributing biases

Comparing two datasets is necessarily insufficient to identify which of the two has a systematic error (or bias) as compared to the truth. However, the use of several datasets, combined with results from prior assessments, can be of assistance to gain additional knowledge. We hereby illustrate how. Using a variety of observation data, Simmons et al. (2014) point out a moist bias in the tropical upper troposphere in the ERA-Interim background. Using SSM/T-2 radiances, this moist bias is confirmed here in Figs. 6(b) and 7(b), where the centre of distribution is located slightly off the diagonal to the right, meaning that simulations are colder than observations except in the lower part of the distribution.

When the SSM/T-2 measurements are compared with simulations using the JRA-55 profiles, the centre of distribution is located slightly off the diagonal to the left (Fig. 8 (b)), which is the opposite to the case of ERA-Interim. This is due to (and consistent with) the fact that the forecast model used for JRA-55 has a dry bias in the upper and mid troposphere (Kobayashi et al., 2015a).

Average departures of SSM/T-2 from reanalyses depend on the biases of the reanalyses used as references. The following subsection focuses the assessment on the stability of biases and inter-satellite biases.

5.3. Temporal stability of SSM/T-2 measurements

Figs. 9 and 10 show monthly time series for the mean departures from the ERA-Interim analysis and the standard deviations over the tropical ocean for the upper, mid and lower tropospheric humidity channels, and the 150 GHz and 91.655 GHz window channels (channels 2, 1, 3, 5 and 4, respectively). Fig. 11 shows brightness temperatures from SSM/T-2 over the tropical ocean and radiative transfer simulations using ERA-Interim and ERA-20C profiles, to which a 12-month running mean is applied in order to remove seasonal variations for clarity. These time series are computed after excluding poor quality data mentioned in Section 4.2 (i.e., measurements at the scan positions 26–28) and in Section 4.3 (i.e., corrupted data). Here, observations are considered corrupted if absolute values of departures from the ERA-Interim analysis are equal or greater than 20 K for the tropospheric humidity channels (1–3) and 50 K for the window channels (4, 5). Note, the threshold for the window channels is raised compared to that for the tropospheric channels in view of larger standard deviations of departures of the window channels. Although specific quality controls for geolocation errors (Section 4.1) are not performed here, most severely affected observations along shorelines in the window channels are removed by the departure check.

5.3.1. Upper tropospheric humidity channel (2)

For DMSP 11, monthly mean departures from the ERA-Interim analysis towards the end of the data record are about 0.5 K smaller than in the beginning (Fig. 9(a)). For DMSP 12, monthly mean departures exhibit a decreasing trend from the beginning of the data record to the end of 2000, and then show a sharp drop of about 0.5 K. Monthly mean departures of DMSP 14 show a similar drop at the same time, but otherwise they are generally stable. Time series for 12-month running mean brightness temperatures (Fig. 11(a)) show that simulations using ERA-Interim profiles rise by 0.5 K around that time; this coincides with the first assimilation of brightness temperatures from AMSU-B in ERA-Interim in October 2000 (Dee et al., 2011, Figure 14; Poli, 2010). On the other hand, we observe no comparable variation at that time in either observations or simulations using ERA-20C profiles (Fig. 11(a)); ERA-20C was produced assimilating only surface observations. Therefore, the sharp drop around end of 2000 is most likely due to the introduction of AMSU-B to ERA-Interim, thereby constraining better the moist bias therein in the tropical upper troposphere. For DMSP 15, monthly mean departures rise suddenly again by 0.5 K in the year 2003. Thereafter they exhibit a positive trend, which is not seen in the other satellites. It should be noted that standard deviations of DMSP 14 increase after the year 2001 (Fig. 10(a)).

DMSP 12 and 14 collected observations at almost the same local time (around 20:50) in mid-1999. During this orbital overlapping period, the representation of the diurnal cycle in the validating reanalyses has little impact on estimation of inter-satellite biases. There is a steady difference of about 1 K between departures of DMSP 12 and 14 including in the orbital overlapping period, which suggests a continuous inter-satellite bias between these two satellites. Using the transformation method of Buehler and John (2005) for the upper tropospheric humidity channel

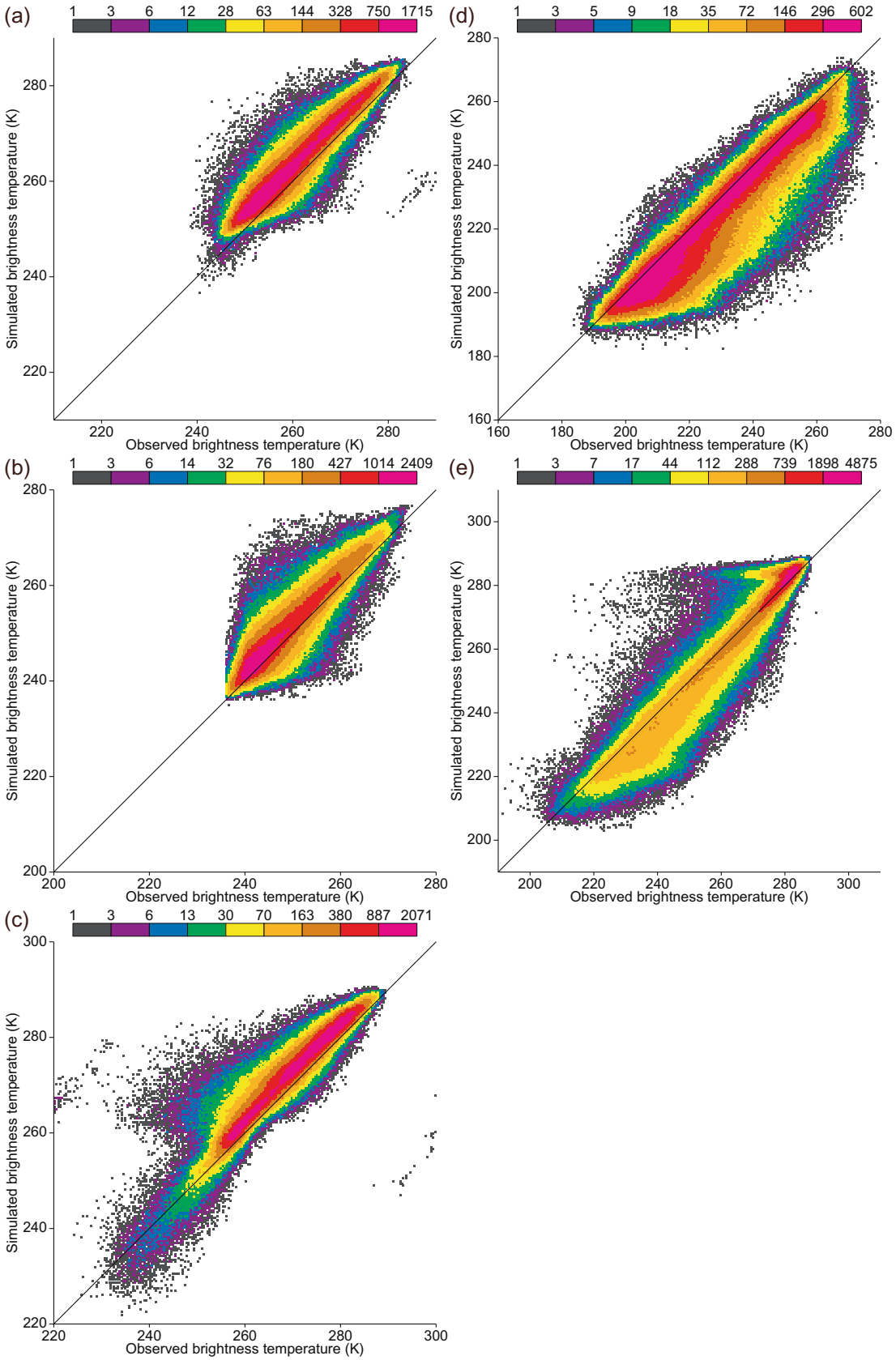

Fig. 8. As Fig. 7, but using JRA-55 profiles instead of ERA-Interim profiles as input to the radiative transfer simulations.

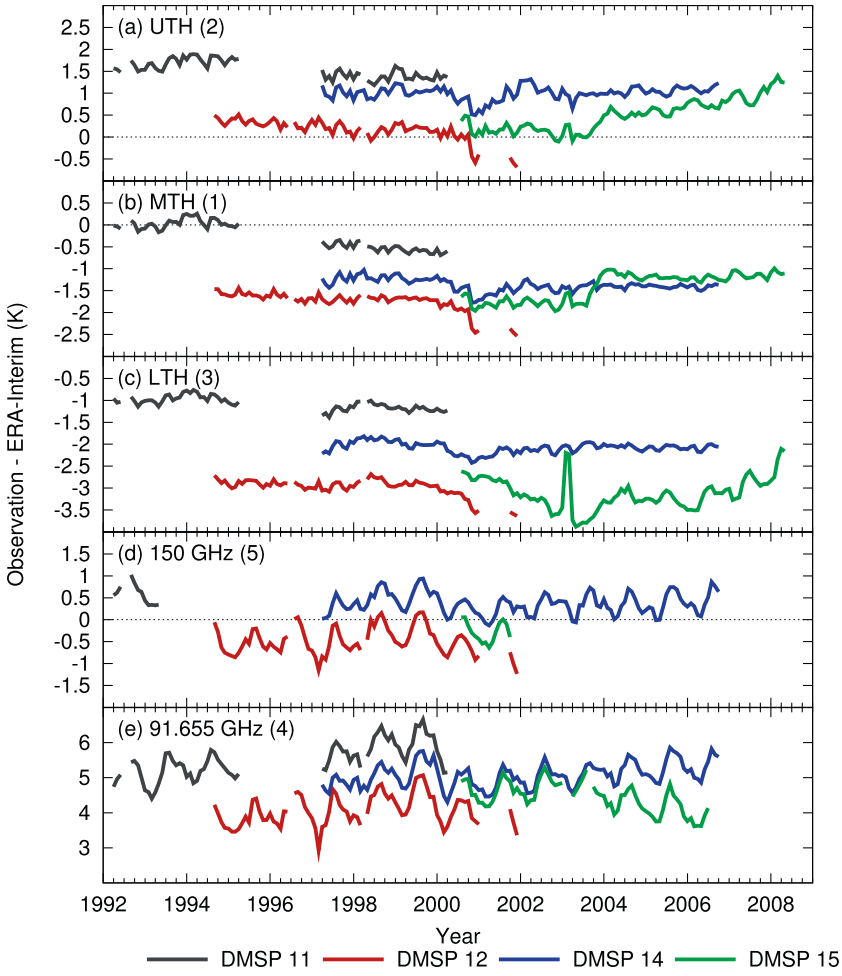

Fig. 9. Monthly mean departures from the ERA-Interim analysis averaged over the tropical ocean (30°N to 30°S) for (a) channel 2 (UTH), (b) channel 1 (MTH), (c) channel 3 (LTH), (d) channel 5 (150 GHz) and (e) channel 4 (91 GHz). The statistics are computed using clear-sky data only.

(2), the difference of 1 K in brightness temperature should correspond to a difference of around 2% in relative humidity. Since this magnitude exceeds inter-annual variations, it is essential to correct for such inter-satellite biases before using these data directly in climate applications. In a reanalysis data assimilation application, such biases may be estimated and corrected automatically by a variational bias correction, using all the information sources available (e.g., Dee et al., 2011).

5.3.2. Mid tropospheric humidity channel (1)

Similarly to the upper tropospheric humidity channel (2), it can be seen in Fig. 9(b) that monthly mean departures of DMSP 11 are about 0.5 K smaller in the second half of the record as compared to the first half; there is a continuous inter-satellite bias of about 0.5 K between DMSP 12 and 14; DMSP 15 exhibits a sudden jump of about 0.5 K in the year 2003. It should be noted that there is a difference of about 0.5 K between brightness temperatures simulated from ERA-Interim for DMSP 12 and 14 (Fig. 11(b)), which in theory should be computed from the same profiles and agree with each other during the orbital overlapping period in mid-1999. This indicates that there is a difference between cloud detection rates of these two satellites, most likely due to inter-satellite biases in the mid and upper tropospheric humidity channels (1, 2), which are used for the cloud filtering. It could also be argued that even within the data record of a single satellite, variations in biases cause variations in cloud detection rates, resulting in spurious trends in simulated brightness temperatures. For simulations using the ERA-Interim and ERA-20C profiles, DMSP 14 and 15 drift apart from 2000 to 2006, whereas for observations, they do not during this period. This is most likely due to a positive trend in biases in the mid and upper tropospheric humidity channels (1, 2) for DMSP 15 (Fig. 9(a) and (b)). The positive trend in biases in these channels results in an increase in the number of observations passing the cloud detection. Those additional observations represent measurements likely under wetter conditions, for which the corresponding radiative transfer simulations produce colder brightness temperatures. It is thus important to correct for such biases in order to maintain consistency of cloud filtering across multiple satellites and throughout the data record of each satellite.

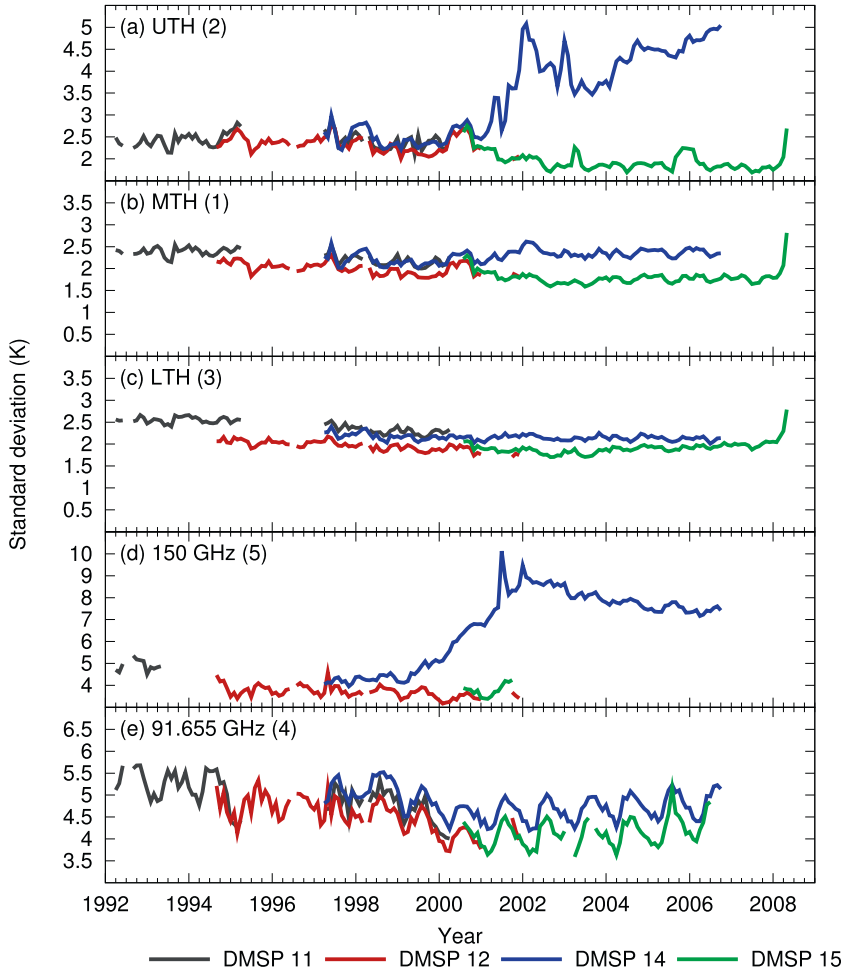

Fig. 10. As Fig. 9, but for standard deviation.

Fig. 11(b) indicates that ERA-20C shows a smaller positive trend in brightness temperature space than ERA-Interim. This result is consistent with ERA-20C having a more balanced water cycle, with precipitation minus evaporation fluctuating around zero on yearly time-scales (Poli et al., 2016).

Consistent with Fig. 11(a), Fig. 11(b) indicates that, at any given time, the inter-satellite spread is generally smaller for all simulations from ERA-20C than from ERA-Interim. If this spread is due to differences between the satellite sampling local times, and thus reflects the diurnal cycle of water vapour, this remark would tend to indicate that ERA-20C has a weaker diurnal cycle in humidity than ERA-Interim. Because the inter-satellite spread in observations is influenced by more effects than just diurnal cycle, it is impossible to conclude at this point which of ERA-20C and ERA-Interim has the more realistic diurnal cycle in humidity.

5.3.3. Lower tropospheric humidity channel (3)

Figs. 9(c) and 11(c) show features similar to those of the mid tropospheric humidity channel (1). The earlier remark about smaller inter-satellite spreads in ERA-20C compared to ERA-Interim is even more visible, suggesting that the amplitude of the differences does come the diurnal cycle amplitude, with greater water vapour amounts, hence variations, in the lowest-peaking channel.

In addition, there is a spike in monthly mean departures of DMSP 15 from February to March 2003. The source of the spike is most likely observations from DMSP 15 since the spike appears only in time series for monthly mean brightness temperatures from DMSP 15, not in time series for monthly mean simulations using either ERA-Interim or ERA-20C profiles, when a 12-month running mean is not applied to them (not shown). DMSP 15 departures exhibit a positive trend after 2003, which is not seen in any other satellite.

5.3.4. 154 Ghz channel (5)

For this channel, measurements from DMSP 11 appear to be unusable after 20 June 1993, most likely due to failure of the 75 GHz Gunn diode oscillator (Kieu et al., 1994). In addition, for the same channel, measurements from DMSP 15 are unstable after November 2001. All these measurements are excluded from the statistics shown in Figs. 9 and 10. Note, DMSP 14 exhibits increase of standard devi-

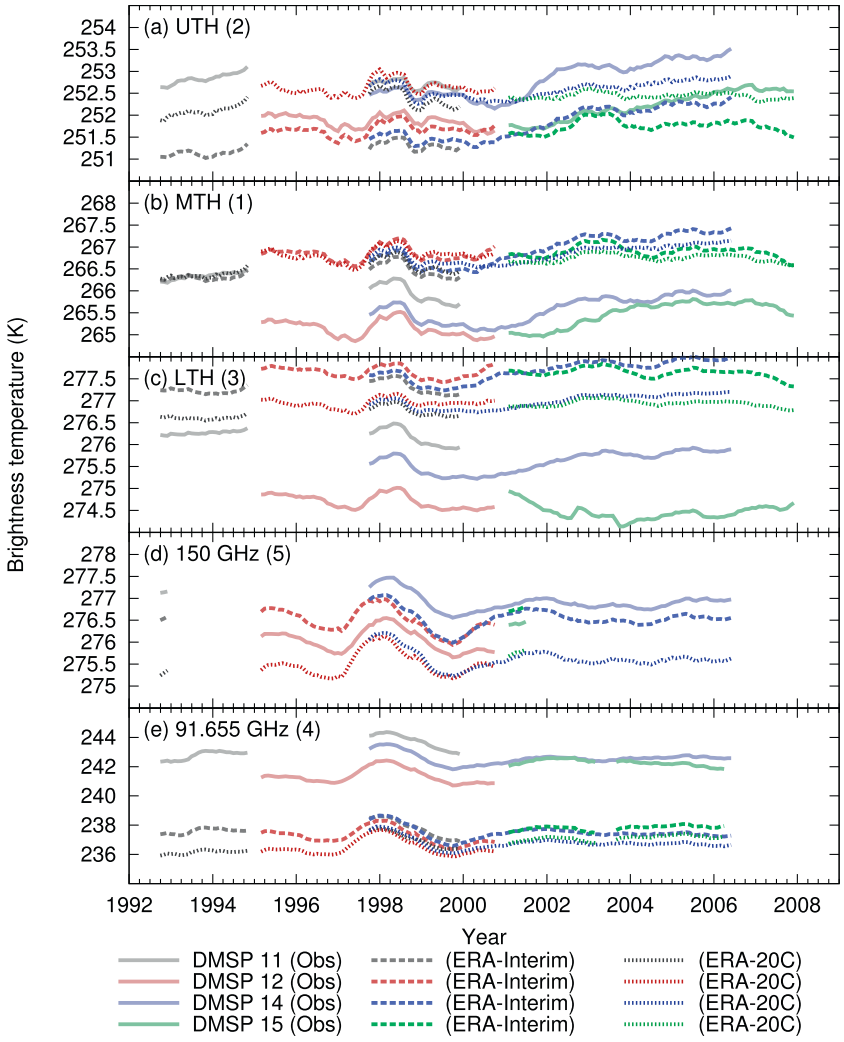

Fig. 11. 12-month running mean brightness temperatures from SSM/T-2 and radiative transfer simulations using ERA-Interim and ERA-20C profiles averaged over the tropical ocean (30°N to 30°S). The statistics are computed using clear-sky data only.

ations after 1999. After excluding these data, few stable measurements are available, covering only a limited period, which limits their value for application to long-term climate monitoring.

5.3.5. 91.655 Ghz channel (4)

Monthly mean departures from the ERA-Interim reanalysis for this channel show generally increasing trends, except DMSP 15, which exhibits a decreasing trend (Fig. 9(e)). Monthly mean departures of both DMSP 12 and 14 fall by about 0.5 K (Fig. 9(e)) and standard deviations decrease by about 0.5 K early in 2000 (Fig. 10(e)). This change comes from an increase in brightness temperatures simulated from ERA-Interim profiles (Fig. 11(e)). That increase is most likely due to an increase in the sea surface temperature (SST) forcing of ERA-Interim, which used a variety of datasets over its record (Dee et al., 2011). This is with contrast to ERA-20C, which used a single, a priori temporally consistent, SST forcing, and shows a more modest increase than ERA-Interim around the year 2000.

It should be noted that measurements from DMSP 15 are of degraded quality after 14 August 2006 due to interference from a radar calibration beacon (http://nsidc.org/data/docs/daac/f15_platform.gd.html), which also affected the SSM/I instrument on the same platform (Hilburn and Wentz, 2008). For this reason, the SSM/T-2 measurements from DMSP 15 are excluded from the statistics after this date.

6. Conclusions and recommendations

In this study, SSM/T-2 radiances are characterised using radiative transfer simulations from global atmospheric reanalyses. The results confirm that the SSM/T-2 measurements between 1992 and 2008 are reasonably stable, and so they should be considered for climate applications, given the availability of similar measurements from nearly 20 other 183 GHz sounders thereafter, such as AMSU-B, SSMIS, MHS, MWHS, MTVZA-GY, ATMS, the *Sondeur Atmosphérique du Profil d'Humidité Intertropicale par Radiométrie* (SAPHIR; Roca et al., 2015), and the Global

Precipitation Measurement (GPM) Microwave Imager (GMI; Draper et al., 2015). Note that more SSM/T-2 data may be available back to 1991 and after 2008. The study has also revealed issues that need to be taken into account before producing a radiance FCDR from the SSM/T-2 measurements, or before assimilation into future climate reanalyses.

For the radiative transfer model, the polarisation state of the SSM/T-2 is examined by comparing observations and simulations for the window channels. The result confirms the conclusion of Burns et al. (1998), i.e., the SSM/T-2 antenna was very likely oriented towards horizontal polarisation in the limit of nadir viewing.

The departures of channel 4, which has a large sensitivity to the surface, reveal that DMSP 14 suffers from large geolocation errors. For SSM/I on DMSP satellites, Berg et al. (2013) corrected geolocation errors using more accurate spacecraft ephemeris and sensor mounting angles estimated from differences between brightness temperatures of ascending and descending orbits to produce FCDRs from these data. A similar method should be explored to address the geolocation errors in SSM/T-2 data. Also, satellite zenith angles are computed from nominal nadir angles and the Earth's radius as an ellipsoid of revolution because the SSM/T-2 input data record does not contain this information. Recalculation of geolocation could be the occasion to derive more accurate satellite zenith angles.

The measurements at three outermost positions (26–28) on the solar side of the SSM/T-2 on DMSP 11, 14 and 15 are seriously contaminated by the glare obstruction bracket, which was designed to keep sunlight out of the instrument cavity (e.g. Miao et al., 2001). Unless a correction method based on physical principles can be derived, these data should be excluded from further production of the FCDR and use in reanalyses. It could be valuable to construct a computer model of the DMSP spacecraft and conduct graphical ray-tracing simulations as done by Kunkee et al. (2008b). This may give further insights regarding inter-satellite differences.

The brightness temperatures during the period before 1994 contain unphysical values quasi-periodically. Quality flags in the SSM/T-2 data record are not necessarily set for these poor quality data. Therefore, additional quality control such as a departure check is necessary to remove them.

To detect cloud-affected measurements, the cloud filtering method of Buehler et al. (2007) for AMSU-B is employed. In the scatter density plots between observed and simulated brightness temperatures, the data after the cloud filtering are in general distributed along the diagonal. However, departures from the diagonal suggest that the cloud filtering method needs to be improved. For reanalysis applications, an all-sky assimilation scheme, which explicitly takes into account the scattering effect of hydrometeors in radiative transfer simulations, is also worth consideration. In addition, simulated brightness temperatures for the 91.655 GHz channel are considerably lower than observations, indicating that radiances from the surface are underestimated in the radiative transfer simulations.

Stability of SSM/T-2 measurements is assessed using time series for brightness temperatures and their departures averaged over the tropical ocean. For the tropospheric humidity channels (1–3) of SSMT-2 on DMSP 11, monthly mean departures from the ERA-Interim analysis show a decreasing trend (about 0.5 K in total over the record length). Monthly mean departures of DMSP 12 and 14 are in general stable, but there is a steady difference of 0.5–1 K in all channels between them, including during the orbital overlapping period when the two satellites made observations at almost the same local times. This indicates that continuous inter-satellite biases exist between the two satellites. The magnitude of this bias for the upper tropospheric humidity channel (2), at about 1 K in brightness temperature or around 2% in relative humidity, exceeds inter-annual variations. This mandates correction of biases before using these data directly in climate monitoring applications. Reanalyses may be able to exploit the data with the help of automated or variational bias correction methods that use the other observations available to discriminate between sources of systematic error.

It should be noted that the results obtained in this study are relevant to the antenna temperatures. Availability of antenna pattern correction data and relative contributions of antenna patterns to the systematic error should also be investigated.

For the channels 2 and 5 of SSM/T-2 on DMSP 14, standard deviations of departures increase after 2001 and 1999 respectively. The measurements from DMSP 15 are unstable for all channels after November 2001 when the measurements of channel 5 degrade significantly. Therefore, caution is needed when using the measurements after this date from DMSP 15 for climate monitoring and reanalyses. We hope that the findings summarised here will eventually enable the generation of a 183 GHz FCDR from SSM/T-2 and the assimilation into future reanalyses.

Acknowledgements

This study was made possible by the EUMETSAT Satellite Application Facility on Climate Monitoring (CM SAF) visiting scientist programme for Shinya Kobayashi's visit and the respective affiliation institutions of the authors. Computing facilities were provided by ECMWF. Prior to this study, SSM/T-2 data were obtained from NOAA NGDC. Support towards the creation of a SSM/T-2 FCDR was partially provided by the European Union Seventh Framework Programme (EU FP7) projects ERA-CLIM (Grant agreement no. 265229) and ERA-CLIM2 (Grant agreement no. 607029). Peter Rayer and the EUMETSAT NWP SAF are thanked for providing radiative transfer coefficients for SSM/T-2. The authors would also like to thank Roger Saunders and William Ingram for advice during the course of this study.

Appendix A. Blacklisted periods

The present appendix summarizes the parts of the SSM/T-2 radiance data record that are not used in this study, due to quality issues:

- SSM/T-2 on DMSP 11: Channel 5 after 20 June 1993, most likely due to failure of the 75 GHz Gunn diode oscillator (Kieu et al., 1994).
- SSM/T-2 on DMSP 15: All channels from 25 December 2000, 21 UTC to 26 December 2000, 21 UTC, due to large noise; Channel 5 after November 2001, due to unstable radiances; Channel 4 from February to March, and in September 2003, due to large noise; Channel 4 after 14 August 2006, due to interference from a radar calibration beacon (http://nsidc.org/data/docs/daac/f15_platform.gd.html).

References

Berg, W., Sappiano, M.R.P., Horsman, J., et al., 2013. Improved geolocation and earth incidence angle information for a fundamental climate data record of the SSM/I sensors. IEEE Trans. Geosci. Remote Sens. 51, 1504–1513. http://dx.doi.org/10.1109/TGRS.2012.2199761.

Buehler, S.A., John, V.O., 2005. A simple method to relate microwave radiances to upper tropospheric humidity. J. Geophys. Res. 110, D02110. http://dx.doi.org/10.1029/2004JD005111.

Buehler, S.A., Kuvatov, M., Sreerekha, T.R., et al., 2007. A cloud filtering method for microwave upper tropospheric humidity measurements. Atmos. Chem. Phys. 7, 5531–5542. http://dx.doi.org/10.5194/acp-7-5531-2007.

Burns, B.A., Wu, X., Diak, G.R., 1998. Impact of emissivity model errors on retrieval of water vapor profiles over ocean with SSM/T2. In: 1998 IEEE International Geoscience and Remote Sensing Symposium Proceedings. Seattle, USA, 6–10 July 1998, pp. 2171–2174. http://dx.doi.org/10.1109/IGARSS.1998.703776.

Chen, K., English, S., Bormann, N., et al., 2015. Assessment of *FY-3A* and *FY-3B* MWHS observations. Weather Forecast. 30, 1280–1290. http://dx.doi.org/10.1175/WAF-D-15-0025.1.

Chung, E.-S., Soden, B.J., Huang, X., et al., 2016. An assessment of the consistency between satellite measurements of upper tropospheric water vapor. J. Geophys. Res. Atmos. 121, 2874–2887. http://dx.doi.org/10.1002/2015JD024496.

Dee, D.P., Uppala, S.M., Simmons, A.J., et al., 2011. The ERA-Interim reanalysis: configuration and performance of the data assimilation system. Q. J. R. Meteorol. Soc. 137, 553–597. http://dx.doi.org/10.1002/qj.828.

Draper, D.W., Newell, D.A., Wentz, F.J., et al., 2015. The Global Precipitation Measurement (GPM) Microwave Imager (GMI): instrument overview and early on-orbit performance. IEEE J. Sel. Top. Appl. 8, 3452–3462. http://dx.doi.org/10.1109/JSTARS.2015.2403303.

Falcone, V.J., Griffin, M.K., Isaacs, R.G., et al., 1992. SSM/T-2 calibration and validation data analysis. Environ. Res. Papers, 1111, Phillips Laboratory, Hanscom Air Force Base, USA.

Felde, G.W., Pickle, J.D., 1995. Retrieval of 91 and 150 GHz Earth surface emissivities. J. Geophys. Res. 100 (D10), 20855–20866. http://dx.doi.org/10.1029/95JD02221.

Ferraro, R.R., Weng, F., Grody, N.C., et al., 2000. Precipitation characteristics over land from the NOAA-15 AMSU sensor. Geophys. Res. Lett. 27, 2669–2672. http://dx.doi.org/10.1029/2000GL011665.

Galin, I., Brest, D.H., Martner, G.R., 1993. The DMSP SSM/T-2 microwave water-vapor profiler. SPIE Proc. 1935, 189–198. http://dx.doi.org/10.1117/12.152603.

GCOS, 2010. Implementation plan for the global observing system for climate in support of the UNFCCC (2010 update). GCOS Rep. 138, 186p. Available online at <www.wmo.int/pages/prog/gcos/Publications/gcos-138.pdf>.

Gorobets, N.N., Cherny, I.V., Chernyavsky, G.M., et al., 2007. Microwave Imager/Sounder *MTVZA-GY* of spacecraft "Meteor-M". In: MSMW'07 Symposium Proceedings. Kharkov, Ukraine, June 25–30. 2007, pp. 772–774. http://dx.doi.org/10.1109/MSMW.2007.4294809.

Hartmann, D.L., Klein Tank, A.M.G., Rusticucci, M., et al., 2013. Observations: atmosphere and surface. In: Stocker, T.F., Qin, D., Plattner, G.-K. (Eds.), Climate Change 2013: The Physical Science Basis. Contribution of Working Group I to the Fifth Assessment Report of the Intergovernmental Panel on Climate Change. Cambridge University Press, Cambridge, United Kingdom and New York, NY, USA.

Hilburn, K.A., Wentz, F.J., 2008. Mitigating the impact of RADCAL beacon contamination on F15 SSM/I ocean retrievals. Geophys. Res. Lett. 35, L18806. http://dx.doi.org/10.1029/2008GL034914.

John, V.O., Chung, E.-S., 2014. Creating a microwave based FCDR for tropospheric humidity: Initial assessment of SSM/T-2 radiances. Global Space-based Inter-Calibration System (GSICS) Quarterly, Special Issue on Microwave, vol 8. http://dx.doi.org/10.7289/V55H7D64.

John, V.O., Holl, G., Allan, R.P., et al., 2011. Clear-sky biases in satellite infrared estimates of upper tropospheric humidity and its trends. J. Geophys. Res. 116, D14108. http://dx.doi.org/10.1029/2010JD015355.

Kakar, R.K., 1983. Retrieval of clear sky moisture profiles using the 183 GHz water vapor line. J. Climate Appl. Meteorol. 22, 1282–1289. http://dx.doi.org/10.1175/1520-0450(1983)022<1282:ROCSMP>2.0.CO;2.

Kieu, D., Stogryn, A., Goe, G., et al., 1994. The performance of the SSM/T-2 moisture sensor on DMSP S12: Part II: Post-June 1993 anomaly. SPIE Proc. 2222, 45–54. http://dx.doi.org/10.1117/12.178024.

Kobayashi, S., Ota, Y., Harada, Y., et al., 2015a. The JRA-55 reanalysis: general specifications and basic characteristics. J. Meteorol. Soc. Jpn. 93, 5–48. http://dx.doi.org/10.2151/jmsj.2015-001.

Kobayashi, S., Poli, P., John, V., 2015b. CM-SAF Visiting Scientist Activity CM_VS14_01 Report: Characterisation of SSM/T-2 radiances using ERA-Interim and other reanalyses. ERA Report Series. 21. ECMWF. UK. 37p. Available online at <http://www.ecmwf.int/sites/default/files/elibrary/2015/10518-cm-saf-visiting-scientist-activity-cmvs1401-report-characterisation-ssmt-2-radiances-using.pdf>.

Kunkee, D.B., Poe, G.A., Boucher, D.J., et al., 2008a. Design and evaluation of the first Special Sensor Microwave Imager/Sounder. IEEE Trans. Geosci. Remote Sens. 46, 863–883. http://dx.doi.org/10.1109/TGRS.2008.917980.

Kunkee, D.B., Swadley, S.D., Poe, G.A., et al., 2008b. Special Sensor Microwave Imager Sounder (SSMIS) radiometric calibration anomalies-Part I: Identification and characterization. IEEE Trans. Geosci. Remote Sens. 46, 1017–1033. http://dx.doi.org/10.1109/TGRS.2008.917213.

Liu, Q., Weng, F., English, S.J., 2011. An improved fast microwave water emissivity model. IEEE Trans. Geosci. Remote Sens. 49, 1238–1250. http://dx.doi.org/10.1109/TGRS.2010.2064779.

Lu, Q., Bell, W., Bauer, P., et al., 2011. Characterizing the FY-3A microwave temperature sounder using the ECMWF model. J. Atmos. Ocean. Technol. 28, 1373–1389. http://dx.doi.org/10.1175/JTECH-D-10-05008.1.

Lu, Q., Bell, W., 2014. Characterizing channel center frequencies in AMSU-A and MSU microwave sounding instruments. J. Atmos. Ocean. Technol. 31, 1713–1732. http://dx.doi.org/10.1175/JTECH-D-13-00136.1.

Miao, J., Kunzi, K., Heygster, G., 2001. Atmospheric water vapor over Antarctica derived from Special Sensor Microwave/Temperature 2 data. J. Geophys. Res. 106 (D10), 10187–10203. http://dx.doi.org/10.1029/2000JD900811.

Moradi, I., Meng, H., Ferrano, R.R., et al., 2013. Correcting geolocation errors for microwave instruments aboard NOAA satellites. IEEE Trans. Geosci. Remote Sens. 51, 3625–3637. http://dx.doi.org/10.1109/TGRS.2012.2225840.

Poli, P., 2010. List of observations assimilated in ERA-40 and ERA-Interim (v1.0). ERA Report Series, 4, ECMWF, UK, 25p. Available online at <http://www.ecmwf.int/sites/default/files/elibrary/2010/11692-list-observations-assimilated-era-40-and-era-interim-v10.pdf>.

Poli, P., Peubey, C., Fennig, K., et al., 2015. Pre-assimilation feedback on a Fundamental Climate Data Record of brightness temperatures from Special Sensor Microwave Imagers: A step towards MIPs4Obs? ERA Report Series. 19. ECMWF. UK. 50p. Available online at <http://www.ecmwf.int/sites/default/files/elibrary/2015/11695-pre-assimilation-feedback-fundamental-climate-data-record-brightness-temperatures-special.pdf>.

Poli, P., Hersbach, H., Dee, D., et al., 2016. ERA-20C: An atmospheric reanalysis of the twentieth century. J. Climate 29, 4083–4097. http://dx.doi.org/10.1175/JCLI-D-15-0556.1.

Robel, J. (ed.), 2009. NOAA KLM user's guide with NOAA-N, -N' supplement. February 2009 revision, NOAA, USA. Available online at <http://www.ncdc.noaa.gov/oa/pod-guide/ncdc/docs/klm/index.htm>.

Roca, R., Brogniez, H., Chambon, P., et al., 2015. The Megha-Tropiques mission: a review after three years in orbit. Front. Earth Sci. 3, 17. http://dx.doi.org/10.3389/feart.2015.00017.

Saunders, R., Hocking, J., Rundle, D., et al., 2013. RTTOV-11 science and validation report. EUMETSAT NWP SAF, 62p. Available online at <http://nwpsaf.eu/site/software/rttov/documentation/>.

Simmons, A.J., Poli, P., Dee, D.P., et al., 2014. Estimating low-frequency variability and trends in atmospheric temperature using ERA-Interim. Q. J. R. Meteorol. Soc. 140, 329–353. http://dx.doi.org/10.1002/qj.2317.

Stickler, A., Grant, A.N., Ewen, T., et al., 2010. The Comprehensive Historical Upper-Air Network. Bull. Am. Meteorol. Soc. 91, 741–751. http://dx.doi.org/10.1175/2009BAMS2852.1.

Weng, F., Zou, X., Sun, N., et al., 2013. Calibration of Suomi national polar-orbiting partnership advanced technology microwave sounder. J. Geophys. Res. 118, 11187–11200. http://dx.doi.org/10.1002/jgrd.50840.

Wessel, J.E., Boucher, D., 1998. Comparison between cross-track and conical scanning microwave window channels near 90 GHz. IEEE Trans. Geosci. Remote Sens. 36, 16–24. http://dx.doi.org/10.1109/36.655314.

WMO, 2016. OSCAR/Space. <https://www.wmo-sat.info/oscar/spacecapabilities> (accessed 15 October 2016).